ORIGINAL PAPER

An analytical model to determine the impact force of drone strikes

Florian Franke[1,2] · Michael Schwab[2] · Uli Burger[2] · Christian Hühne[1,3]

Abstract

In addition to the well-known threats of bird and hail strikes, small unmanned aerial vehicles (sUAV) pose a new threat to manned aviation. Determining the severity of collisions between sUAVs and aircraft structures is essential for the safe use and integration of drones in airspace. A generic analytical calculation model needs to be developed to supplement the existing test and simulation data. This paper presents an analytic model for drone collisions with perpendicular and inclined targets. The targets have a rigid or elastic material behavior. The aircraft impact model, which is used for the design of nuclear reactor structures, is transferred and adjusted for sUAV impacts to calculate the impact force. A mass- and a burst load distribution are needed as input parameters. Both distributions are determined for an sUAV design depending on the flight direction. Compared to previous calculations, the new approach is to consider a moving target structure, which produces more realistic results. We compare the calculation results with simulation data from sUAV collisions with a commercial airliner windshield from the literature. The calculations show plausible results and a good agreement with literature data. Subsequently, the influence of the input parameters on the impact force is investigated. We see that spring stiffness, target mass, burst load distribution and damping have minor influence on the overall impact force. The impact velocity, mass distribution and flight orientation on the other hand have a major influence on the impact force. Further tests are needed to validate the impact model.

List of symbols

α	Flight orientation	l	Length of one UAV arm
γ	Inclination around y-axis	l_i	Length of single components
ζ	Inclination around z-axis	m	Mass
μ	Mass per unit length	m_c	Crushed mass
ν	Poisson's ratio	m_i	Mass of single components
ρ	Density	m_{li}	Mass along one UAV arm
σ_y	Yield strength	n	Number of drone components
F	Impact force	t	Time
L	Projectile length	v_i	Initial velocity
M	Target mass	v_t	Target velocity
P	Burst load	x	Position along the projectile
c	Target damping	x_{li}	Position along one UAV arm
k	Target spring stiffness	y	Target displacement
		z	Projectile displacement
		$x_a; y_a; z_a$	Target coordinate system

Abbreviations

AIM	Aircraft impact model
ASSURE	Alliance for System Safety of UAS through Research Excellence
CAA	Civil Aviation Authority
CASA	Civil Aviation Safety Authority

✉ Florian Franke
Florian.Franke@thi.de

1   TU Braunschweig, Brunswick, Germany

2   Technische Hochschule Ingolstadt, Ingolstadt, Germany

3   Deutsches Zentrum für Luft- und Raumfahrttechnik, IAF, Brunswick, Germany

DJI	Da-Jiang Innovations Science and Technology Co., Ltd
EASA	European Union Aviation Safety Agency
FEA	Finite element analysis
LiPo	Lithium-polymer
MTOW	Maximum take-off weight
NRC	National Research Center of Canada
PC	Polycarbonate
PU	Polyurethane
Pvb	Polyvinyl butyral
RPAS	Remotely piloted aerial system
sUAV	Small unmanned aerial vehicle
UAS	Unmanned aerial system
UAV	Unmanned aerial vehicle

1 Introduction

The use of small unmanned aerial vehicles (sUAV) increases. An unmanned aerial vehicle (UAV) with a maximum take-off weight (MTOW) of less than 25 kg is a small UAV (sUAV) [1]. SUAVs are also known under the terms drones, UAS (unmanned aerial system) or RPAS (remotely piloted aerial system). There will be more than 67 Million deliveries of non-military drones worldwide in 2021 [2]. Drones operate in the most diverse areas. We use them for photos, videos, traffic monitoring, farming and further leisure activities. Future applications like parcel delivery services are under investigation. This growth also increases the risk of a collision between manned aircraft and sUAV. This development can be seen in Germany, for example. The number of near encounters between manned and unmanned aircraft in the airspace of Germany grew from 14 in 2015 to 158 in 2018 according to the German Air Traffic Control [3]. Similar developments can be observed in countries all over the world, e.g. in Great Britain [4]. The unknown threat of sUAVs to manned aviation also leads to severe economic damage. Drone sightings forced different airports to close. For example, London Gatwick was shut down for 2 days in December 2018.

We use the definition of a drone strike from [5]. A "drone strike" describes a collision of an UAV with a manned aircraft. Collisions between drones and aircraft have not yet been fully investigated. There are only a few studies on this topic so far. The Civil Aviation Safety Authority (CASA) analyzed the damage potential of drone strikes [6]. They calculated the penetration speed of different materials subjected to drone strikes. The airframe of a commercial airliner will penetrate if the impact speed is higher than 103 m/s, independent of the drone size [6]. The Bard Institute published a drone impact and ingestion study in 2015 [7] based on the work conducted by CRASH Lab. One conclusion from their finite element analysis (FEA) is that drones with a MTOW between 1.0 and 3.0 kg can cause critical damage to aircraft structures. The "Alliance for System Safety of UAS through Research Excellence" (ASSURE) published an "UAS Airborne Collision Severity Evaluation" [8] with corresponding technical volumes [1, 9, 10]. They performed numerical simulations of drone strikes on different aircraft types (business jet, commercial airliner) and aircraft components (windshield, horizontal stabilizer). They validated their simulations with impact tests of drone components against different targets. Their conclusion is that a drone impact will cause more damage than bird strikes for the same amount of kinetic energy. The Civil Aviation Authority (CAA) determined that helicopters have a higher risk of mid-air collisions with sUAVs and structural damage than fixed wing aircraft [11]. The European Union Aviation Safety Agency (EASA) categorized drones with a MTOW beneath 25.0 kg. They are categorized into the four categories "Harmless", "Small", "Medium", and "Large" [12]. Song and Schroeder investigated the ingestion of an sUAV into high-bypass engines [13–15]. They concluded that drones pose a greater level of threat than current certification specifications allow [14]. Meng et al. [16] conducted impact tests and simulations with a DJI (Da-Jiang Innovations Science and Technology Co., Ltd) Inspire 1 drone on a horizontal stabilizer of a commercial airliner. According to their research, a commercial plane cannot safely continue its flight after a drone strike. Lu et al. [17] investigated the collision safety between an aircraft windshield and five different drones. They performed simulations and compared the results with full scale collision tests. They conclude that a DJI Phantom 4 with a mass of 1.4 kg may initiate severe damage at an impact velocity of 154.8 m/s.

All previous mentioned studies have in common that none of them deal with the analytic modeling of the force during the collision. An analytical model can be used for the preliminary design of structures and thus save costs for simulations and experiments. This paper presents an analytical model to determine the impact force during a drone strike. The basic calculation model is described within chapter 2. Chapter 3 presents the calculation results on different targets and compares the results with data from the literature. The influence of various parameters on the impact force is investigated within this chapter. We discuss the findings and the model within chapter 4.

2 Models for calculation of impact forces due to drone strikes

None of the current models for calculation of impact load cases for the design of aeronautical structures is valid for drone strikes. The bird strike model from Wilbeck assumes that the missile behaves like a fluid [18]. The hail strike

impact model is strain rate dependent and assumes a fluid behavior after the internal stresses of the projectile reach the strength of ice [19]. Both models assume that the projectile behaves like a fluid. Since a drone consists of several solid bodies, however, these models cannot be transferred to a drone strike. Instead, the following approach is based on the aircraft impact model (AIM) by Riera [20]. This model was originally developed to design nuclear reactors against aircraft crashes.

2.1 Basic aircraft impact model for rigid targets

The basic idea of the aircraft impact model is that the impacting mass of the projectile (drone) m reduces during the impact duration by its crushed mass m_c (Fig. 1). The whole drone decelerates during the impact process.
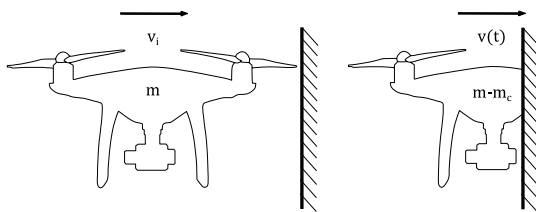
Fig. 1 Principal drone strike on a rigid target according to the aircraft impact model [5]

The basic aircraft impact model is a one-dimensional impact calculation model. It considers the aircraft as a line with a defined mass and burst load distribution [21]. These two distributions will be described in chapter 2.3 and 2.4. The advantage of this approach over previous impact models is, that the impact of several bodies can be represented. This model divides the projectile into two areas, a crushed and a rigid uncrushed zone. The whole projectile structure has a perfectly plastic behavior. Figure 2a shows the basic aircraft impact model on a rigid target. The part of the drone mass that impacts the target (crushed zone) is dm. The crushed mass does not sum up at the target. The force $F(t)$ during impact time can be calculated by Eq. 1 [20]:

$$F(t) = P(x(t)) + \mu(x(t))(dx/dt)^2 \qquad (1)$$

The burst load distribution is $P(x)$, $\mu(x)$ is the mass distribution, while $x(t)$ is the position along the projectile. The burst load P and the mass per unit length μ have to be determined. Both depend on the position x along the structure and the current flight orientation of the sUAV. The derivative dx/dt is the velocity difference between the target velocity $\vec{v}_t$ and the projectile velocity $\vec{v}$ [22].
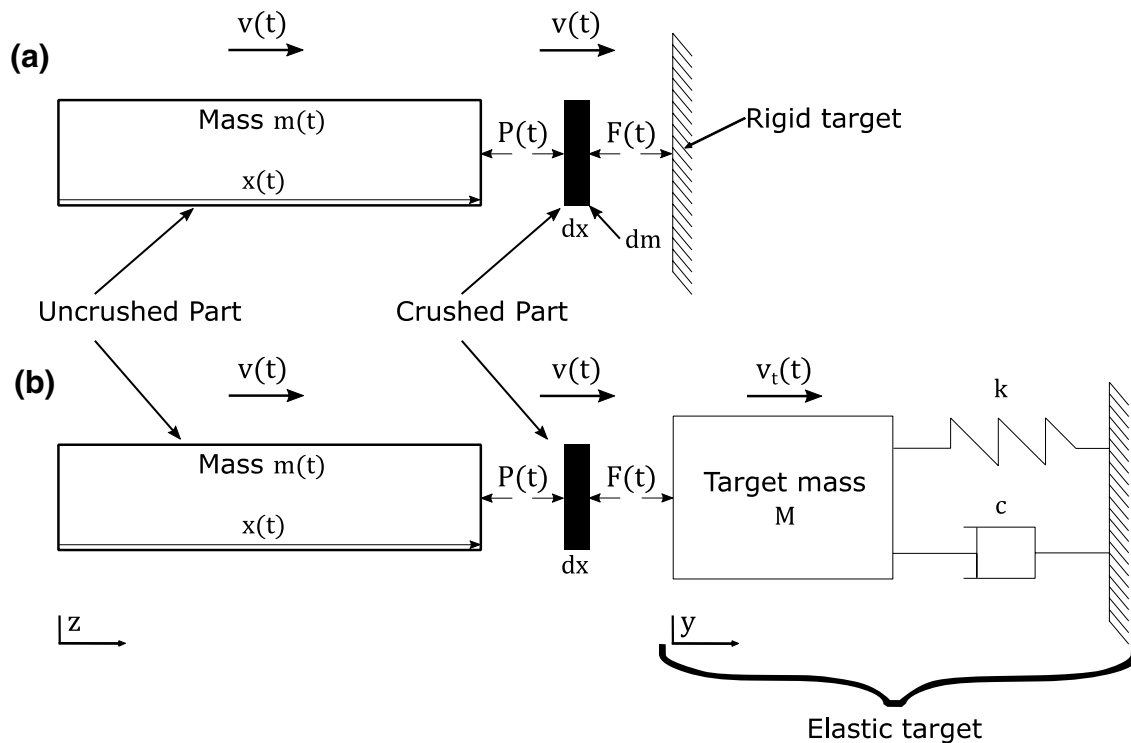

Fig. 2 **a** Aircraft impact model for rigid targets; **b** aircraft impact model for elastic targets; adapted from [22]

2.2 Impact model for elastic targets

Other authors (Wolf et al. [23], Laczák et al. [22]) extended the model to calculate more realistic, elastic targets. They model the target as a spring damper system (Fig. 2b). The following differential equations Eq. 2 and Eq. 3 are obtained. They can be used together with Eq. 1 to determine the impact force [22]:

$$\frac{d^2x}{dt^2} = \frac{P(x(t))}{m(t)} + \frac{d^2y}{dt^2} \tag{2}$$

$$\frac{d^2y}{dt^2} = \frac{P(x(t))}{M} + \frac{\mu(x(t))}{M}\left(\frac{dx}{dt}\right)^2 - \frac{c}{M} \cdot \frac{dy}{dt} - \frac{k}{M}y(t) \tag{3}$$

The mass of the target is M, c is the target damping constant and k is the target spring constant. The current mass of the projectile is $m(t)$. The mass- and burst load distributions of the drone μ and P are also used here. They will be described in the following chapters. If the target is rigid, Eq. 3 equals 0. The initial conditions are [22]:

$$x(0) = L; \frac{dx}{dt}(0) = -v_i \tag{4}$$

$$y(0) = 0; dy/dt(0) = 0 \tag{5}$$

with L as the length of the projectile. v_i is the initial velocity of the projectile.

2.3 Mass distribution

The "Phantom 4" by DJI (DJI P4) is the most sold UAV within the open category [24]. It is a quadcopter with four motors. It has a MTOW of 1380 g according to [25]. Its maximum velocity is 20 m/s [25]. The method to get the mass distribution is to simplify the whole drone model to a 1-D line model in flight direction. Figure 3a shows this simplification process for the aircraft impact model, Figs. 3b and c shows it for a drone strike. To get the mass distribution, we use the reverse engineering method. That means, we disassemble the drone, weigh every component and divide this by the length of the specific component. The overall mass distribution $\mu(x)$ is the sum of all component mass distributions at their positions along the projectile length L (Eq. 6):
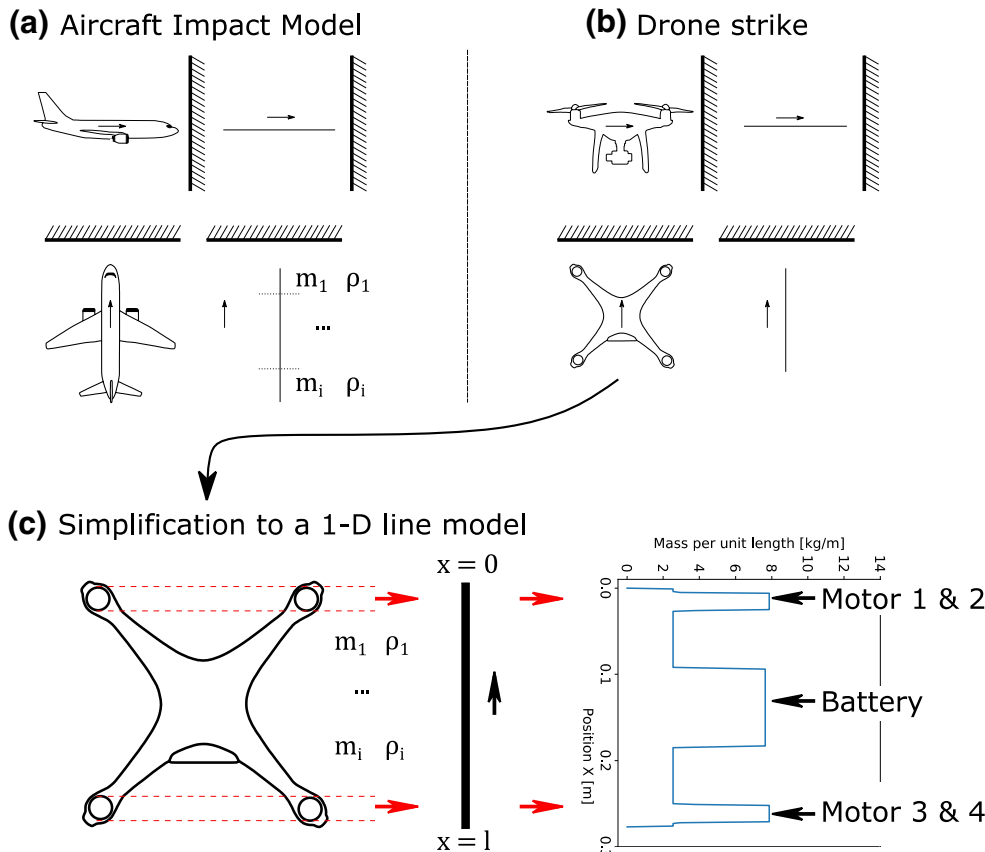

Fig. 3 Simplification of the sUAV to a 1-D line model and method for determining the mass per unit length μ

Table 1 Measured masses and lengths of DJI P4 components used to calculate the basic mass distribution μ independent of flight orientation α

	UAV	Shell	Battery	Motor
Mass [g]	1387	713	454	55
Length [mm]	393	393	128	28
μ [g/mm]	3.53	1.81	3.54	1.96

Table 2 Material values for determination of basic burst load distribution

Component	Material	Crushing force [N]
Shell	Polycarbonate	$0.6346 \cdot (x \cdot 10^3 \text{ mm})^2$
Battery	Lithium-polymer	5000
Motor	AA 5754-H111	12,546

$$\mu(x) = \frac{m}{L(x)} = \sum_{i=1}^{n} \frac{m_i}{l_i(x)} \qquad (6)$$

With n as the number of drone components, l_i as the component length, and m_i as the mass of the component. This value is applied at the position of the components. We may plot the results over the whole projectile length and see the mass distribution $\mu(x)$. Figure 3c visualizes this method. Heavy individual components of the drone lead to deflections in the mass distribution. Deflections in the mass distribution due to the motors and the battery are marked as examples in the figure. The landing gear, payload as well as the electrical systems are disregarded. Rather, the mass of these components is evenly applied to the shell mass. We assume that none of the parts break away before they impact the target.

Table 1 summarizes the masses and lengths of a reverse engineered DJI P4 and its components. This table presents the mass and length of one motor. Using these input parameters, the mass distributions are calculated as a function of the flight orientation.

2.4 Burst load distribution

The other term of the aircraft impact approach is the burst load P. It is also referred to as crushing force. The burst load describes the load bearing capacity of the projectile structure. This function depends on the load and its direction, material, component design and its mode of failure. Every component of the sUAV has a specific burst load. Only shell, battery and motors are investigated. We simplify these components for determining their crushing loads. The motor is simplified to a cylinder out of cast aluminum (AlMg3). The battery is a rectangular solid, which consists of lithium-polymer (LiPo). The drone shell is simplified to a hollow truncated cone out of polycarbonate (PC). This simplification leads to a function of x for the area and the crushing force. Table 2 presents the values for the burst load. The payload, electrical systems, sensors and rotors are neglected. The components fail when their crushing force is reached. The values for polycarbonate and cast aluminum AA 5754-H111 (AlMg3) are based on the material (yield) strength

($\sigma_{PC} = 50$ MPa—rounded off—[26]; $\sigma_{\text{AlMg3}} = 170$ MPa [27]), because the failure during the real load case cannot be predicted without full scale impact tests. The material yield strengths are multiplied with the component areas to determine the crushing force. Preliminary pressure tests show that the battery system of the sUAV has a crushing force of $5000N$. The advantage of the model is that the only material parameter required is the yield stress. If the burst load distribution is determined, for example, via buckling loads, further material parameters are required. However, since the burst load at high impact velocities only has a small share in the total force, as it will be shown later, other forms of failure are not considered in this study.

2.5 Variation of the mass- and burst load distribution with the flight orientation

Quadcopter drones are able hover and to rotate 360 degrees around their vertical axis in flight. Mass and burst load distribution depend on the flight orientation.

We define the flight orientation as the angle α between the velocity vector $\vec{v}$ and one arm of the drone (Fig. 4). It varies between 0° and 45°. To determine the distributions as a function of angle α, the drone may be simplified to a line model with two perpendicular lines. The lines are symmetrical. We calculate the results exemplarily for 0°, 15°, 30° and 45° flight orientation of the sUAV. The length of one quadcopter arm is l. Mass and burst load distribution are determined along this length. Both distributions are symmetrical to the intersection of the perpendicular lines. The basis for angle dependency is the mass and burst load distribution of one arm along its entire length. Trigonometric relationships convert both distributions to a line in flight direction. That is the calculated part of the line model (Fig. 4b). The algorithm mirrors the calculation used to determine the distribution over the entire projectile length.

The sum of the mass distributions of the sUAV arms in relation to the flight direction is the total mass distribution. Since the mass is a scalar, only the length being considered changes. Thus, the total mass is constant. The mass of the motor is considered along its diameter. The two-dimensional diagonal of the rectangular battery case defines the mass per unit length of the battery. Figure 5 shows the determination of the total mass distribution. In

Fig. 4 Simplified sUAV quad-copter model; **a** top view of the sUAV with the corresponding flight direction; **b** simplified line model with angle α
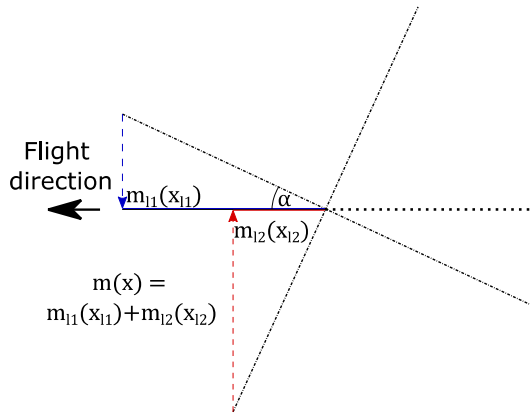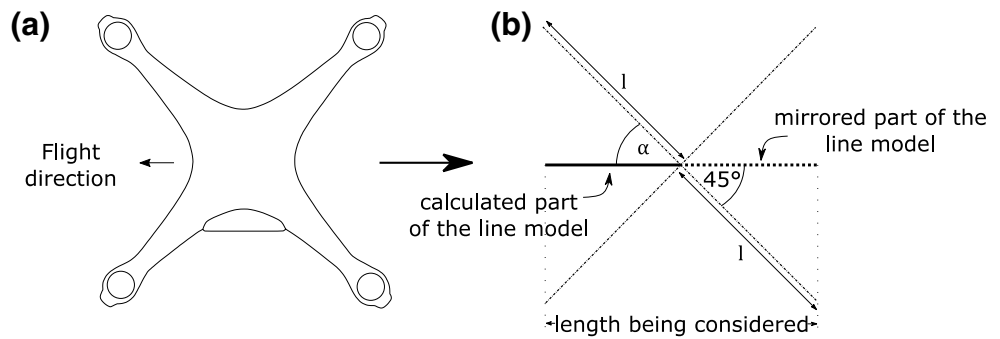

Fig. 5 Determination of mass distribution in dependency of the flight orientation
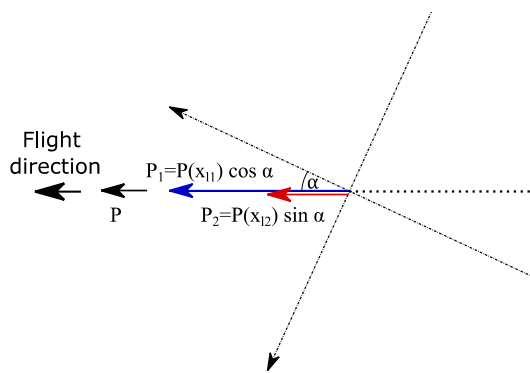

Fig. 6 Determination of burst load distribution in dependency of the flight orientation

contrast, the burst load is a vector. The burst load function only includes the proportion of the burst load vector in flight direction within the following calculations (Fig. 6). Equations 7 and 8 show the extensions for the angle dependency for both distributions. This line model works with angles greater than 0° up to 45° and can thus, due to the symmetry of the geometry, depict all flight orientations of the drone.

$$m(x) = m_{l1}\left(x_{l1}\right) + m_{l2}\left(x_{l2}\right); x_{l2} \geq l \cdot (\cos\alpha - \sin\alpha) \qquad (7)$$

$$P(x) = P\left(x_{l1}\right) \cdot \cos\alpha + P\left(x_{l2}\right) \cdot \sin\alpha \qquad (8)$$

Figure 7 shows mass- and burst load distributions for different flight orientations. Figure 7a shows the mass- and burst load distribution for a 45° flight angle. The mass distribution (see Eq. 6) along the length being considered has three peaks of approximately the same height. The burst load shows three load peaks as well. The battery in the middle of the sUAV defines the greatest load peak. This peak load is two times higher than the other two. These are in turn determined by the motor. With a 45° orientation, two motors are at the same position along the length being considered (e.g., Figure 3c). With decreasing angles, the positions of the motors change. This leads to further peaks in the mass- and burst load distributions (Fig. 7b and c for 30° and 15°). At a flight orientation of 15° the masses of two motors and the battery overlap. This leads to high peaks in the mass distribution, (Fig. 7c). In the burst load function, this superposition is not as pronounced. The usage of trigonometric relationships leads to a singularity for the 0° flight orientation. To avoid this singularity at 0°, the detailed mass- and burst load distributions are used. If we integrate the mass distributions over the relevant length, the results equal the total mass of the sUAV. The integral of the burst load is inconstant due to the directional dependency.

3 Calculation results

We use the 4th order Runge–Kutta method to solve the differential equations by numerical integration, as it is done by Laczák [22]. The calculation stops when either $v(t) = 0$ m/s or $x(t) = 0$ m. The impact force drops to zero at this point. We use a Python script for all calculations. We investigate impacts on perpendicular and inclined as well as rigid and elastic targets.

The target structure is inclined around the y_a-axis by 45° (γ) and around the z_a-axis by 25° (ζ), (Fig. 8). The
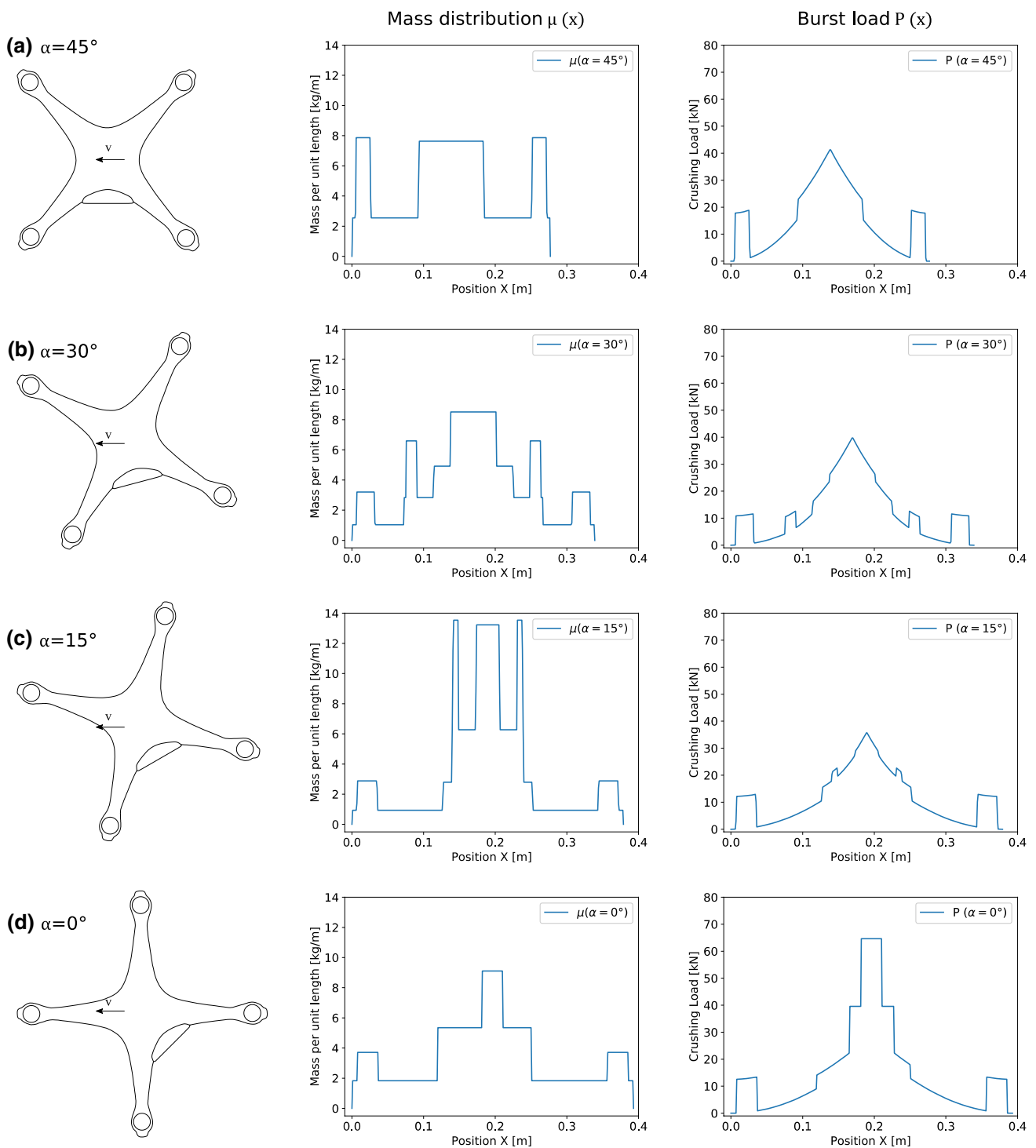
Fig. 7 Mass- and burst load distribution for different flight orientations α; **a** 45°, **b** 30°, **c** 15°, **d** 0° [5]

geometry configuration of a commercial airliner windshield is the basis for these inclinations. We compare our calculation results with FE impact simulation on aircraft windshield from Lu et al. [17]. Their windshield model has a thickness of $h = 22.5$ mm. It consists out of five layers and three materials (Inorganic glass, polyurethane (PU) and

polyvinyl butyral (Pvb)). The material data used by Lu et al. are shown in Table 3. We model the windshield in a simplified way using mass, spring stiffness and damping as shown in Fig. 2b. The used parameters are explained in chapter 3.2. The influence of the individual parameters on the impact force is investigated in chapter 3.4.
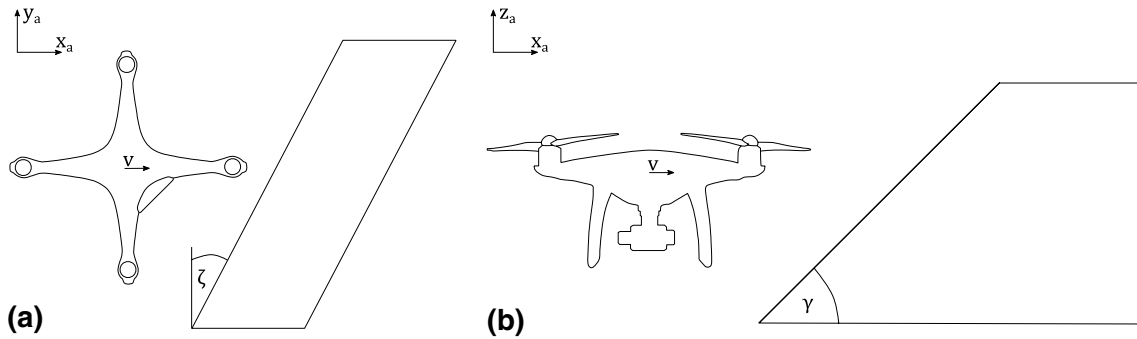
Fig. 8 Definition of inclination angles **a** ζ (z_a-axis); **b** γ (y_a-axis) [5]

Table 3 Material properties of the windshield used by Lu et al. [17]

	Inorganic glass	PU	Pvb
Density ρ [kg/mm^3]	2.45e–6	1.0e–6	1.0e–6
Young's modulus E [GPa]	71.48	0.499	1.293
Poisson's ratio ν [−]	0.22	0.3	0.38
Yield stress σ_y [MPa]	370	150	150

To calculate the impact force on an inclined target, we use the following equation (Eq. 9):

$$F(t) = \left(P(x(t)) + \mu(x(t)) \left(\frac{dx}{dt} \right)^2 \right) \cdot \sin(\gamma) \cdot \cos(\zeta) \qquad (9)$$

The angles act only on the impact force $F(t)$. The inclination also has an influence on the burst and mass distribution, which is neglected for initial calculations. We calculate the impact force–time results for all flight and target orientations with Eqs. 1–3, and Eq.9. The initial impact velocity of the sUAV is $v_i = 154.8$ m/s, according to [17]. The timestep size for numerical integration is set to $\Delta t = 10^{-6} s$.

3.1 Impact on a stationary rigid target with varying flight orientations

We expect that the course of the impact force over time has several load peaks. These load peaks represent the impact of individual components on the target. The components collide with the target one after the other. Figure 9 shows an exemplary, reasonable force–time curve with assignment of the load peaks to the impacts of the components. We see that the impact of the several components is represented. The order and height of the load peaks correspond to the design and the flight orientation of the drone. First the motors, which are in front in the direction of flight (M1 and M2), hit the target. Then the battery B hits the target. Afterwards the rear motors (M3 and M4) collide with the target. The impact of the battery produces the greatest peak as the battery is
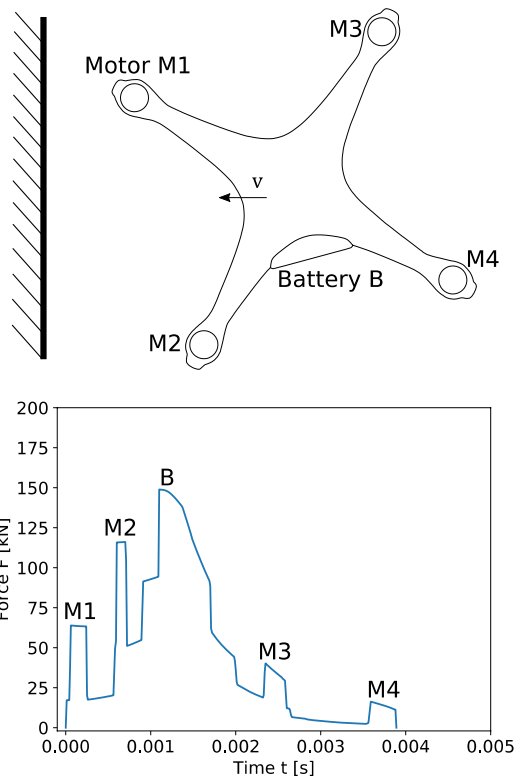

Fig. 9 Exemplary impact force–time course with assignment of the load peaks to the impacts of the components [5]

the heaviest component of the sUAV. The uncrushed part of the projectile becomes smaller and decelerates during the impact process. This leads to a flattening of the curve with increasing time. This shows that this model allows an investigation of the influence of individual components on the overall impact force.

It depends on the flight direction when and whether the individual components hit the target structure. This is more evident in Figs. 10, 11. They present the impact force of a drone strike on perpendicular (Fig. 10) and inclined rigid targets (Fig. 11) for different flight orientations. Figure 10
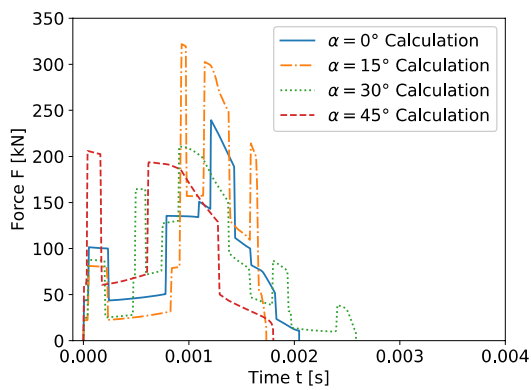
Fig. 10 Calculation results for sUAV impacts with a perpendicular target for varying flight orientations (0°, 15°, 30°, 45°)
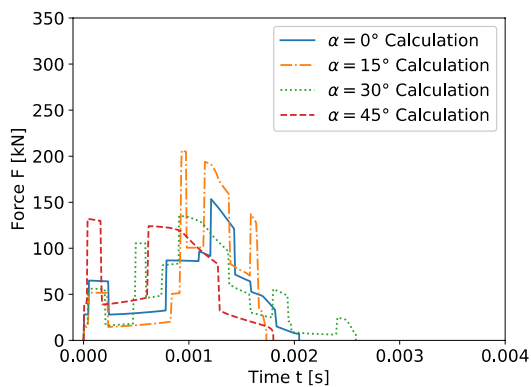

Fig. 11 Calculation results for sUAV impacts with an inclined rigid target for varying flight orientations (0°, 15°, 30°, 45°)

shows the impact force–time curves for flight orientations of 0°, 15°, 30° and 45°. All graphs show that the motors hit the structure 0.1 ms after the start of the impact. With the 45° orientation two motors hit the target simultaneously. For 0°, 15° and 30° the motors hit the target one after the other. After about 1 ms, the battery reaches the target. The battery has the largest mass of all components, which is why this impact produces a great peak load in the overall course. It depends on the effective deceleration whether the rear engines also hit the target. If the termination condition $v(t) = 0$ m/s is reached, there is an uncrushed part of the projectile left which does not hit the target. If the other termination condition $(x(t) = 0)$ is reached, the whole projectile hits the target. The duration of the impact also depends on the deceleration. The impact duration varies between 2.5 ms for the 15° orientation and 3.8 ms for the 30° orientation. A similar course can be seen in Fig. 11 for the inclined impact, only the amplitude is lower due to the inclination angles of the target. Instead of a perpendicular impact, the drone is deflected along the angle of inclination. Decreasing angles of flight orientation lead to higher force peaks due to the simplification of the sUAV as

a line model and the use of trigonometric relationships. The 0° orientation is an exception, as here detailed mass and burst load distributions are used to avoid singularities due to the trigonometric relationships.

We compare these results with drone strike FEA data on a commercial airliner windshield from Lu et al. [17] (Fig. 12). We assume a flight orientation of $\alpha = 0°$ and an initial velocity of $v_i = 154.8$ m/s similar to the literature FE data for comparison. The calculations are compared with simulation data of two impact velocities (152.7 m/s, 154.8 m/s). Lu et al. simulated and tested a full drone including rotors impacting a windshield. As we neglect the rotors in our model, the impact starts therefore with 0.6 ms offset. The calculated impact force shows two load peaks, which can also be seen in the comparative data. The times at which the load peaks of the individual components occur show a slight offset. The first load peak appears at 0.65 ms in the calculation due to the impact of the motor. The first load peak in the FEA result for the windshield appears at 0.7 ms. The maximum load for the analytical determined force appears at 1.9 ms. For the FEA data, the peak load is reached at 1.5 ms. The peak load of the calculation deviates from the maximum load on the windshield by 19.7 % (154.8 m/s) resp. 11.8 % for the impact velocity 152.7 m/s. The impact force of the calculation drops to 0 at 2.7 ms. The impact force of the windshield simulation shows another peak, which starts at 4.0 ms. This deflection is caused by the impact of the rear motor.

We see that the analytical calculation agrees with the simulation data up to 1.5 ms. After this point, the courses diverge. The deviations result from the fact that the comparative results are determined for deformable aircraft structures like the windshield. The analytic model used so far assumes a rigid target structure and a rigid projectile behavior. The FEA also enables more precise, full scale modelling. In contrast, the sUAV is viewed in a highly simplified way as a 1-D line. For example, friction losses and the exact material behavior can be considered within
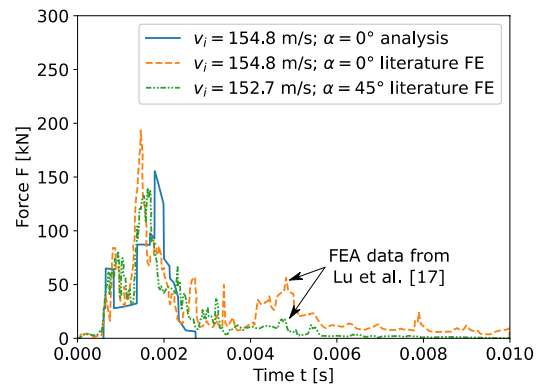

Fig. 12 Comparison of calculation results with FEA simulation data of drone strikes from the literature [17]

Table 4 Input values for impact on elastic targets

Target mass M	Target stiffness k [N/m]	Target damping c [kg/s]	Drone flight orientation α [°]
$10 \cdot m$	1e7	0	0;45

Table 5 Initial conditions for elastic, stationary targets

| $dx/dt(0)$ [m/s]	$dy/dt(0)$ [m/s]	$x(0)$ [m]	$y(0)$ [m]
−154.7	0	L	0

the FEA, whose influence is unrepresented in the analytical model. Furthermore, the analytical model lacks strain rate hardening effects. The AIM assumes that all components are destroyed during impact, which is correct for a full scale aircraft impact due to the large kinetic energy. The impact energies of a drone strike are significantly lower due to the low mass of a drone. Therefore, not all components are completely destroyed. Heavy and dense components (e.g., motors) tend to show plastic deformations rather than fragmentation. Together with the other simplifications such as the neglection of individual components (rotors, camera, circuit board), this leads to further deviations.

The target structure in a mid-air drone strike is not rigid. It is deformable. Therefore, the results in Fig. 12 only serve as a first estimation of the potential of the model. To obtain results that are more in line with reality, the following calculations are performed with the model for elastic target structures (Fig. 2b).

3.2 Drone strike on resting elastic targets

The input values for the impact load cases can be found in Table 4. Due to the short impact duration, the target damping constant c is set to 0 for first investigations. For first calculations, the target mass M is assumed to be ten times the initial projectile mass $m = 1387$ g. The target spring constant k is assumed to be 1e7 N/m for first calculations. The flight orientation α equals 0° resp 45°. Table 5 presents the initial conditions. What stands out in the table is that the target velocity $v_t = dy/dt$ is assumed to be 0. This in turn means that the complete velocity as well as the kinetic energy are in the sUAV projectile. The initial velocity of the projectile $v_i = dx/dt = 154.8$ m/s is the same as for impacts on rigid targets.

Figure 13 shows the results for an impact on a perpendicular, elastic, stationary target. The calculation results for drone strikes with inclined, elastic, stationary targets are shown in Fig. 14. When comparing the values with the results from chapter 3.1, hardly any differences can be found
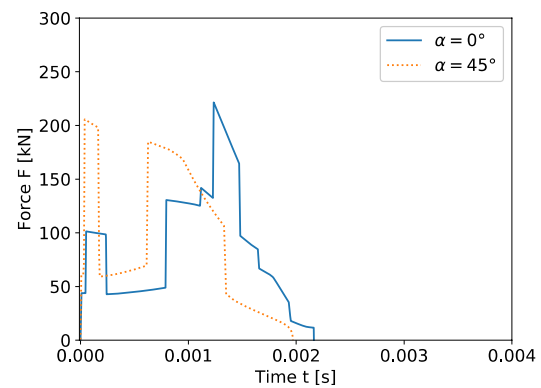
Fig. 13 Calculation results for sUAV impacts with perpendicular, elastic, stationary targets for varying flight orientations
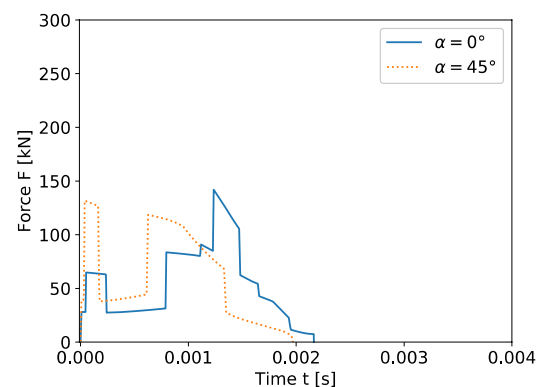
Fig. 14 Calculation results for sUAV impacts with inclined, elastic, stationary targets for varying flight orientations

(Figs. 10, 11), due to the initial conditions and used parameter values.

3.3 Drone strike on moving elastic targets

Previous calculations assume that the sUAV will collide with a resting target. The speed of the overall system only affects the projectile under this assumption. This is incorrect, since a drone has a maximum speed of solely 20 m/s. In addition, the kinetic energy of this assumption deviates from reality. If only the sUAV moves, the influence of the mass and velocity of the target structure is neglected. Therefore, for the following calculations, the speed is distributed according to reality. This means that the drone has a maximum speed of $v_i = dx/dt = 20$ m/s, and the target structure flies at $v_t = dy/dt = 134.8$ m/s towards the projectile. Figure 15 shows the principle velocity distribution during a drone strike. Table 6 lists the input parameters for the following calculations. Table 7 shows the initial conditions.

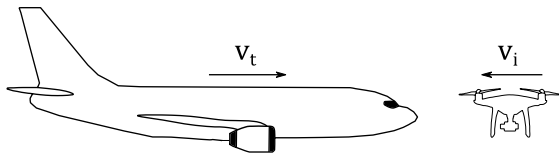Figure 16 presents the calculation results for drone strikes with flight orientations of 0° and 45° on perpendicular,

Fig. 15 Principle velocity distribution during a drone strike [5]

Table 6 Input values for impact on elastic targets

Target mass M	Target stiffness k [N/m]	Target damping c [kg/s]	Drone flight orientation α [°]
$10 \cdot m$	1e7	0	0;45

Table 7 Initial conditions for elastic, moving targets

$dx/dt(0)$ [m/s]	$dy/dt(0)$ [m/s]	$x(0)$ [m]	$y(0)$ [m]
−20	134.7	L	0
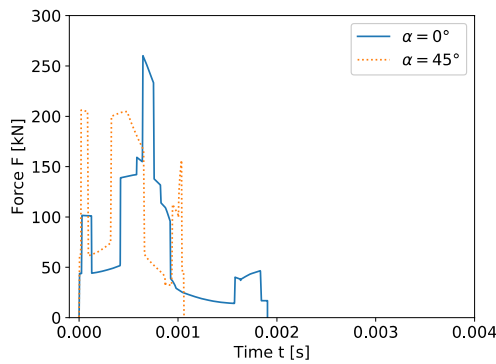
Fig. 16 Calculation results for sUAV impacts with perpendicular, elastic, moving targets for varying flight orientations
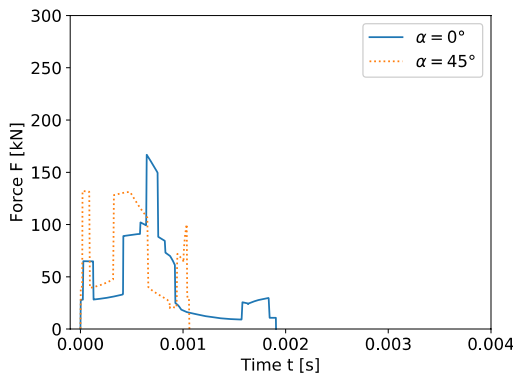
Fig. 17 Calculation results for sUAV impacts with inclined, elastic, moving targets for varying flight orientations
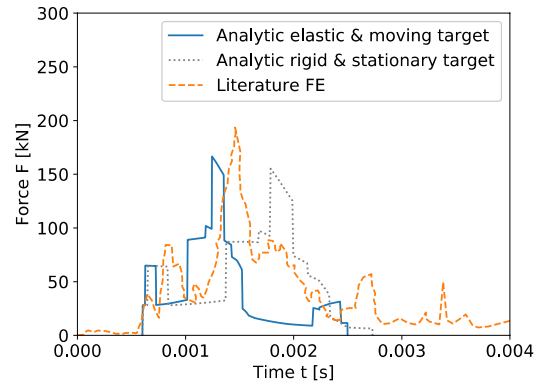
Fig. 18 Comparison of calculation results from different models with FEA data from Lu et al.

elastic, moving targets. Figure 17 shows the force–time curves for impacts on inclined, elastic, moving targets. We see an increase of the magnitude of the peak load compared to the previous calculations by 15.4 %. In contrast to the previous calculations, the rear engines also hit the target for $\alpha = 0°$. This results in a further peak load at the end of the impact. The duration of the load peaks decreases.

Since the considered load case of the moving, elastic target represents reality more closely than a stationary, rigid target, the results are compared here with the FE data (Fig. 18). The force curve changes significantly for the elastic, moving target compared to the stationary, rigid target. The load peak now occurs at $t = 1.2$ ms and is 13.9 % below the FEA data. Figure 18 shows that the total impact duration decreases. This can be explained by the fact that the drone cannot significantly slow down the large target mass during impact. However, in contrast to the impact with a rigid target, there is an impact of the rear motor. In this case, the model for elastic, moving targets can be used to determine the maximum load better than the model for rigid, stationary targets. However, the impact duration decreases, which causes the force curve to deviate strongly from the FE comparison data from 1.5 ms onwards. The following chapter therefore examines how the various parameters influence the force curve.

3.4 Influence of various parameters on the impact force

Within this chapter we investigate the influence of different parameters on the impact force. Only one parameter is varied within the parameter studies. All others are kept constant at the values of Tables 6 and 7.

Figure 19 shows the share of the burst load and mass distribution on the overall impact force for an inclined impact with a 0° flight orientation. The mass distribution has a distinct influence on the overall behavior. This
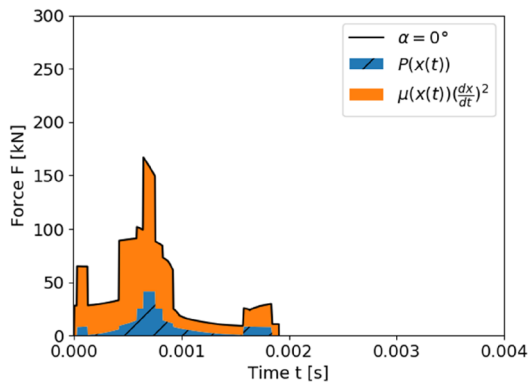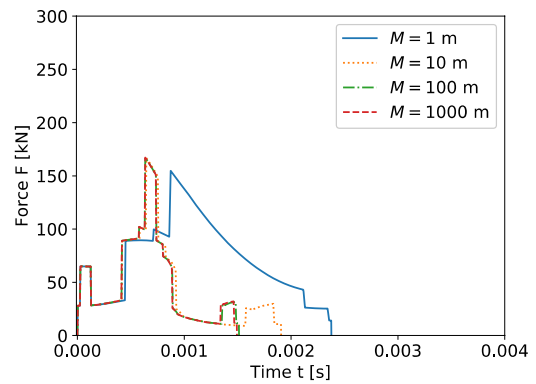
Fig. 19 Share of impact force, $v_t = 134.8$ m/s
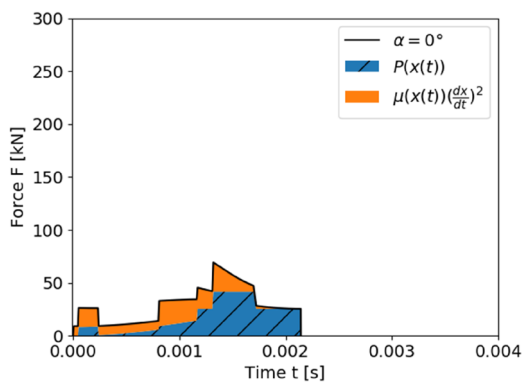

Fig. 21 Variation of target mass M

Fig. 20 Share of impact force, $v_t = 67.4$ m/s

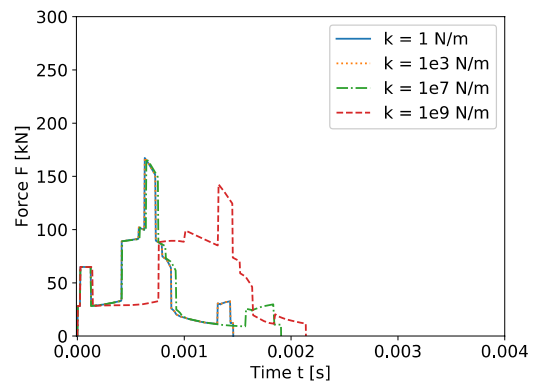**Fig. 22** Variation of target spring constant k

Fig. 23 Variation of target damping constant c

distribution is multiplied by the square of the velocity, which leads to this influence. At the time of the highest total force (166.8 kN), the burst load has a share of 41.4 kN (24.8 %). From this, it can be deduced that the impact force can be changed by adjusting the sUAV component masses and their distribution within the structure. With a lower initial velocity, the share of the burst load in the impact force increases (Fig. 20, v_t reduced by 50 %).

A variation of the target mass is shown in Fig. 21. It can be seen that the force maximum hardly changes. The difference between the maximum load for $M = 1 \cdot$ m and $M = 1000 \cdot$ m is 8.1 %. The impact duration increases with decreasing target mass. A change in the target mass, i.e., the mass of the aircraft, is an unreasonable method of influencing the effects of a drone strike.

A variation of the target spring constant k shows an opposite behavior (Fig. 22). If the constant k increases, the impact duration increases, too. The duration increases by 47.5 %. The peak load decreases by 14.9 %. k represents the stiffness of the target structure. As the duration increases, the force decreases due to the reduction of the projectile deceleration.
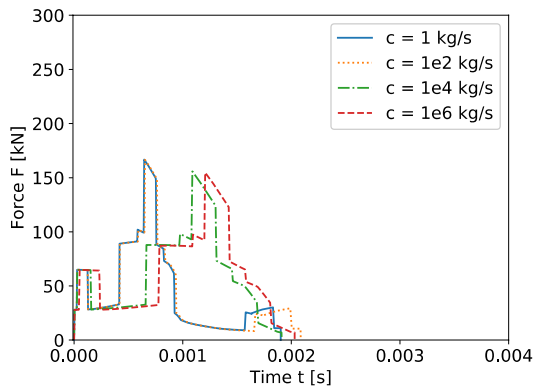
An increase of the target damping constant c has a similar effect as the increase of k (Fig. 23). The impact duration increases by 9.4 % and the peak force decreases by 7.3 %.

We investigate the influence of the projectile velocity. (Fig. 24). We vary v_i between 0 and 30 m/s. The first velocity represents a drone in hover flight. The highest speed (30 m/s) is not reached by DJI Phantom 4 drones so far but the technical development shows an increase in
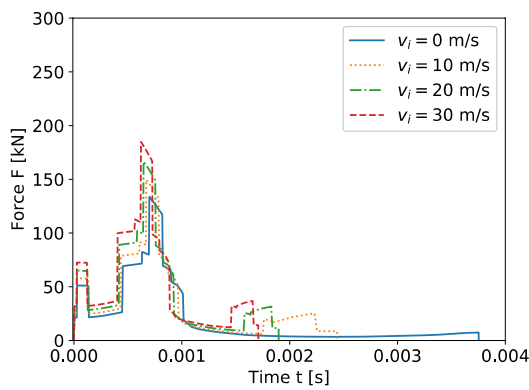
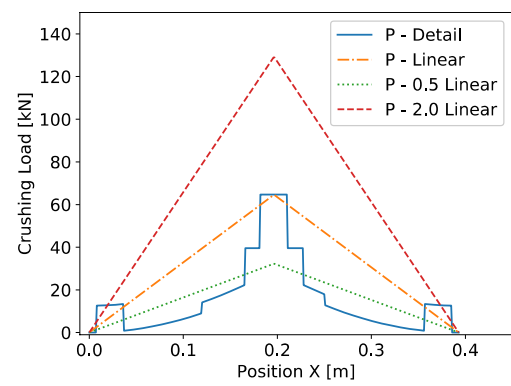**Fig. 24** Variation of projectile velocity v_i

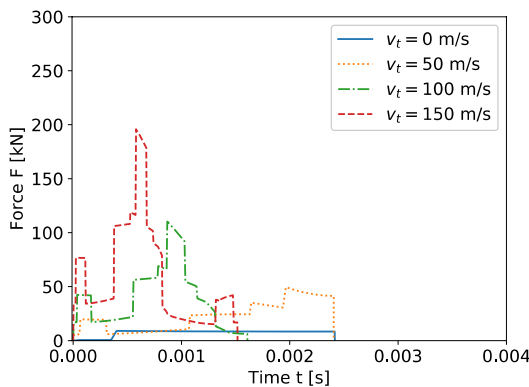**Fig. 26** Variation of burst load distribution $P(x)$

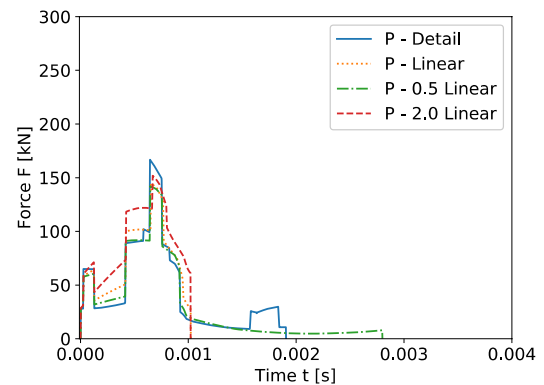**Fig. 25** Variation of target velocity v_t

Fig. 27 Calculation results for different burst load distributions $P(x)$

top speed. This means that this speed may be reached in future UAV designs. A change in projectile velocity from 0 to 30 m/s increases the peak load from 133.8 to 185.1 kN. We see a decrease of the impact duration.

A similar behavior can be observed for the variation of the target velocity (Fig. 25). The largest target velocity shows the highest force peak and the shortest impact duration. A change in the target velocity from 100 to 150 m/s leads to a doubling of the force peak.

We investigate the influence of the burst load. For this, we use the detailed course as well as a linear, 50 % linear and a two times linear distribution (Fig. 26). The linear distribution increases until it reaches the middle of the length being considered. After this point, P decreases. Figure 27 shows the calculations results for the different burst load distributions. We expect that a greater burst load leads to a higher force peak. The results show a lower force peak compared to the detailed distribution (8.9 %) although the burst load is higher. An increase in deceleration can explain this phenomenon. We see a higher force between the end of the impact of the motor ($t = 0.12$ ms) and the beginning of the impact of the battery ($t = 0.41$ ms), which leads to a larger deceleration. The drop of the force to 0 kN

at 1 ms for the linear and two times linear distributions confirms this.

4 Discussion

We see that the presented model is able to calculate impact force–time curves for drone strikes. The original models are developed for rigid and elastic, stationary targets. During impact on elastic targets, we see that the share of the movement of the initial resting target structure in the overall course is negligibly small, due to the mass and spring stiffness. For impact calculations on elastic, resting targets with a mass difference of at least ten times the projectile mass it is therefore advisable to work with the equations for rigid structures.

The comparison with literature FEA data (Fig. 12) shows, that the numerical analysis cannot simulate the force after 3 ms. This is due on the one hand to the termination conditions and on the other hand to the parameter values used. We use the termination conditions according to the literature (Laczák et al. [22]). Their model is originally developed for aircraft impacts. Their assumption, that the

crushing stops either $v(t) = 0$ m/s or $x(t) = 0$ m is valid, as their target structure does not move. For a drone strike, the termination conditions are also valid for stationary targets, e.g., helicopters in hover flight. Current research on drone strikes uses the relative velocity between aircraft and drone for their investigations. While ASSURE [1] and the National Research Center of Canada (NRC) [28] assume that only the drone moves, Lu and Meng [16, 17] assume that the target is moving and the drone is stationary. We follow the first case for the present calculations, whereby the condition $v(t) = 0$ m/s can be fulfilled. It is important to bear in mind that these assumptions are not realistic. In a real drone strike with an aircraft, the speed of the aircraft will be significantly higher than that of the drone. This means that the sUAV will be completely destroyed as the relative velocity cannot drop to 0 m/s in this case. This makes the termination condition $v(t) = 0$ m/s invalid for a real drone strike with an aircraft. This is an important issue for future research.

A reduction of the burst load distribution leads to an increase of the impact duration (Fig. 27). The burst load has a share of about 25 % in the overall impact force for an impact velocity of $v = 154.8$ m/s. A simplified doubling of the burst load distribution leads to a decrease of the force peak by 8.9 %. This results in the possibility to calculate with a simplified distribution in case of unknown burst load distribution without generating a large error. As it can be seen in Figs. 19 and 20 the share of the burst load on the overall force increases with decreasing impact velocity. The determined burst load distributions are based on the material yield strength. The real distribution can deviate from the determined distribution, for example due to strain rate hardening effects or other forms of failure (e.g., buckling). Further forms of failure, like buckling, may be incorporated in the model via the burst load distribution. Since the burst load has only a minor influence on the contact force in the speed range investigated, other forms of failure are not investigated further. Based on these observations, we propose to use a simplified burst load distribution only for impact velocities greater than or equal to 100 m/s.

The parameters M, k and c all have only a minor influence on the maximum force. The principle force–time curves show minor changes. The peak force values decrease by 7.3–14.9 % in the investigated ranges. Only the time at which the maximum force occurs can be changed with these parameters.

A significant change in the impact force is caused by flight orientation, speed and mass distribution. A change in the flight orientation from 45° to 15° may lead to an increase of the peak force by 80 kN. We see, that if an impact is unavoidable, a change in the flight orientation lead to lower impact forces. This opens the opportunity for an optimization of the flight orientation of the sUAV if the impact is unavoidable. 75 % of the overall impact force is determined by the mass distribution multiplied with the squared velocity (Fig. 19). A change in the drone design and the arrangements of the components may lead to a lower impact force. The impact speed has the greatest influence on the force. A change of the target speed from 0 to 150 m/s produces a force ten times greater (Fig. 24).

The presented model is only able to calculate elastic target behavior. It is valid for strong structures that show only minor damage. We are unable to model plastic deformation but it can be expected that hard objects like motors may produce severe local damage and deformations. The plasticity and damage of the target structure will limit the force. This effect is not covered with this calculation model. Furthermore, this model is unable to describe the deformation of the projectile during impact. The model needs detailed mass and burst load distributions to produce good results. In the current form, we assume a rigid projectile, but the sUAV deforms during the impact. We neglect components of the sUAV (e.g., camera, electrical system and landing gear). Instead, we apply their masses evenly along the structure length. The impact model contains no angular momentum. For a full validation, we need impact tests with defined mass- and burst load distributions. This could be the basis for a drone strike substitute structure for further investigations and certification tests.

5 Conclusion

This paper presents a generic analytic approach for determining the impact force of an sUAV collision with an aircraft. This analytic model is developed for varying flight orientations of an sUAV. We present varying mass- and burst load distributions for a DJI Phantom 4, depending on the flight orientation. We show plausible impact force results for perpendicular and inclined targets. Existing analytic models for aircraft crashes lead to reasonable results for drone strikes, compared with drone strike simulation data from the literature. In addition to previous studies, we assume a moving target. This study has found that the calculation model for an elastic, moving target leads to realistic results. The presented model is able to calculate the impact force of a drone strike, if mass- and burst load distribution for the drone projectile are known. The advantage of the model is that the influence of individual components can be investigated via the mass- and burst load distribution. Finally, we discuss the influence of various parameters on the impact force. We found that the mass distribution, flight orientation and velocities have a significant influence on the impact force. The model cannot describe the influence of damage to the target structure on the impact force. A change of the drone design and component arrangement may lead to lower forces. To the best of our knowledge, this study has been

one of the first attempt to develop an analytic approach for impact loads due to drone strikes. Further studies need to be carried out to validate the results by impact tests and to investigate termination conditions for real drone strike scenarios. This model is a pragmatic approach for estimating the loads to be expected in the event of a drone impacting an aeronautical structure as part of a preliminary design.

Declarations

Conflict of interest The authors declare that they have no conflict of interest.

Data availability All relevant data are published within this paper.

Code availability Not applicable.

References

1. Gerardo, O., Gomez, L., Espinosa, J., Baldridge, R., Zinzuwadia, C., Aldag, T.: Volume II—UAS airborne collision severity evaluation. Quadrocopter. UAS airborne collision severity evaluation, 2. FAA, Springfield. http://www.assureuas.org/projects/deliverables/a3/Volume%20II%20-%20UAS%20Airborne%20Collision%20Severity%20Evaluation%20-%20Quadcopter.pdf (2017). Accessed 29 Nov 2017

2. Tractica.: Anzahl weltweit ausgelieferter ziviler Drohnen in den Jahren 2015 bis 2021 (in 1.000). https://de.statista.com/statistik/daten/studie/661094/umfrage/auslieferungen-ziviler-drohnen-weltweit/ (2018)

3. Deutsche Flugsicherung: Sicherheit in der Luftfahrt. Gemeldete Behinderungen des Luftverkehrs durch zivile Drohnen in Deutschland in den Jahren 2015 bis 2019 (2020). Accessed 24 March 2020

4. UK Airprox Board: Drones. UK Airprox Board. https://www.airproxboard.org.uk/Topical-issues-and-themes/Drones/. Accessed 7 January 2020

5. Franke, F., Schwab, M., Burger, U., Hühne, C.: An analytical approach to determine the impact force of small unmanned aerial vehicle collisions with rigid and elastic targets. In: CEAS (ed.) Aerospace Europe conference 2020. Aerospace Europe conference, Bordeaux, 25.-28.02.2020 (2020)

6. Radi, A.: Potential damage assessment of a mid-air collision with a small UAV. Civil aviation safety authority. https://www.casa.gov.au/files/potential-damage-assessment-mid-air-collision-small-rpapdf (2013). Accessed 4 Oct 2016

7. Gettinger, D., Michel, A.H.: Drone sightings and close encounters: an analysis. https://dronecenter.bard.edu/files/2015/12/12-11-Drone-Sightings-and-Close-Encounters.pdf (2015). Accessed 10 May 2021

8. Gerardo, O., Lacy, T., Gomez, L., Espinosa, J., Baldridge, R., Zinzuwadia, C., Aldag, T., Kota, K.R., Ricks, T., Jayakody, N.: UAS airborne collision severity evaluation. Executive summary—structural evaluation. UAS airborne collision severity evaluation. FAA, Springfield. http://www.assureuas.org/projects/deliverables/a3/Volume%20I%20-%20UAS%20Airborne%20Collision%20Severity%20Evaluation%20-%20Structural%20Evaluation.pdf (2017). Accessed 29 Nov 2017

9. Gerardo, O., Lacy, T., Gomez, L., Espinosa, J., Baldridge, R., Zinzuwadia, C., Aldag, T., Kota, K.R., Ricks, T., Jayakody, N.: Volume III—UAS airborne collision severity evaluation. Fixed-wing. http://www.assureuas.org/projects/deliverables/a3/Volume%20III%20-%20UAS%20Airborne%20Collision%20Severity%20Evaluation%20-%20Fixed-wing.pdf (2017). Accessed 29 Nov 2017

10. D'Souza, K., Lyons, T., Lacy, T., Kota, K.R.: Volume IV—UAS airborne collision severity evaluation. Engine ingestion. UAS airborne collision severity Evaluation. FAA, Springfield. http://www.assureuas.org/projects/deliverables/a3/Volume%20IV%20-%20UAS%20Airborne%20Collision%20Severity%20Evaluation%20-%20Engine%20Ingestion.pdf (2017). Accessed 29 Nov 2017

11. David, P.: Drone safety risk: an assessment. CAP 1627. Civil aviation authority, Gatwick (2018). Accessed 11 May 2018

12. European Aviation Safety Agency: Drone collision task force. Final report. European Aviation Safety Agency (2016). Accessed 15 Feb 2017

13. Schroeder, K., Song, Y., Horton, B., Bayandor, J.: Investigation of UAS Ingestion into high-bypass engines, Part 2. Parametric drone study. In: 58th AIAA/ASCE/AHS/ASC structures, structural dynamics, and materials conference. AIAA SciTech Forum. American Institute of Aeronautics and Astronautics (2017)

14. Song, Y., Horton, B., Bayandor, J.: Investigation of UAS ingestion into high-bypass engines, part 1. Bird vs. Drone. In: 58th AIAA/ASCE/AHS/ASC structures, structural dynamics, and materials conference. AIAA SciTech Forum. American Institute of Aeronautics and Astronautics (2017)

15. Song, Y., Schroeder, K., Horton, B., Bayandor, J.: Advanced propulsion collision damage due to unmanned aerial system ingestion. In: 30th Congress of the international council of the aeronautical sciences. 30th Congress of the international council of the aeronautical sciences, Seoul, 25–30.09.2016 (2016)

16. Meng, X., Sun, Y., Yu, J., Tang, Z., Liu, J., Suo, T., Li, Y.: Dynamic response of the horizontal stabilizer during UAS airborne collision. Int. J. Impact Eng. (2019). https://doi.org/10.1016/j.ijimpeng.2018.11.015

17. Lu, X., Liu, X., Li, Y., Zhang, Y., Zuo, H.: Simulations of airborne collisions between drones and an aircraft windshield. Aerosp. Sci. Technol. (2020). https://doi.org/10.1016/j.ast.2020.105713

18. Wilbeck, J.S.: Impact behavior of low strength projectiles. Air Force Materials Lab Wright-Patterson AFB OH (1978)

19. Pernas-Sánchez, J., Pedroche, D.A., Varas, D., López-Puente, J., Zaera, R.: Numerical modeling of ice behavior under high velocity impacts. Int. J. Solids Struct. (2012). https://doi.org/10.1016/j.ijsolstr.2012.03.038

20. Riera, J.D.: On the stress analysis of structures subjected to aircraft impact forces. Nucl. Eng. Des. (1968). https://doi.org/10.1016/0029-5493(68)90039-3

21. Kessler, G., Veser, A., Schlüter, F.-H., Raskob, W., Landman, C., Päsler-Sauer, J.: Belastungsansätze für Flugzeugaufprall. In: Kessler, G., Veser, A., Schlüter, F.-H., Raskob, W., Landman, C., Päsler-Sauer, J. (eds.) Sicherheit von leichtwasserreaktoren: risiken der nukleartechnologie, pp. 183–205. Springer, Berlin (2012)

22. Laczák, L.E., Károlyi, G.: On the impact of a rigid–plastic missile into rigid or elastic target. Int. J. Non-Linear Mech. (2017). https://doi.org/10.1016/j.ijnonlinmec.2017.01.020

23. Wolf, J.P., Bucher, K.M., Skrikerud, P.E.: Response of equipment to aircraft impact. Nucl. Eng. Des. (1978). https://doi.org/10.1016/0029-5493(78)90014-6

24. Skylogic Research: 2018 Drone Market Sector Report. Opportunities and challenges in key market segments. http://droneanalyst.com/research/research-studies/2018-drone-market-sector-report-purchase. Accessed 9 Jan 2019

25. DJI: Phantom 4. Bedienungsanleitung. https://dl.djicdn.com/downloads/phantom_4/de/DE_Phantom_4_User_Manual_v1.2_20160503.pdf (2016)

26. Ultimaker: Technical data sheet PC. https://ultimaker.com/download/74975/UM180821%20TDS%20PC%20RB%20V11.pdf (2018). Accessed 8 Apr 2020

27. Rodriguez-Millan, M., Garcia-Gonzalez, D., Rusinek, A., Arias, A.: Influence of stress state on the mechanical impact and deformation behaviors of aluminum alloys. Metals (2018). https://doi.org/10.3390/met8070520

28. Dadouche, A., Greer, A., Galeote, B., Breithaupt, T., Vidal, C., Gould, R.: Drone impact assessment on aircraft structure: windshield and leading edge testing and analysis, CR-GTL-2020–0054 (2020)